

Spin- S designer hamiltonians and the square lattice $S = 1$ Haldane nematic

Nisheeta Desai and Ribhu K. Kaul

Department of Physics & Astronomy, University of Kentucky, Lexington, KY 40506-0055

(Dated: December 15, 2024)

We introduce a strategy to write down lattice models of spin rotational symmetric Hamiltonians with arbitrary spin- S that are Marshall positive and can be simulated efficiently using world line Monte Carlo methods. As an application of our approach we consider a square lattice $S = 1$ model for which we design a 3×3 - spin plaquette interaction. By numerical simulations we establish that our model realizes a novel “Haldane nematic” phase that breaks lattice rotational symmetry by the spontaneous formation of Haldane chains, while preserving spin rotations, time reversal and lattice translations. By supplementing our model with a two-spin Heisenberg interaction, we present a study of the transition between Néel and Haldane nematic phase, which we find to be of first order.

Introduction: The relationship between lattice spin models and their long distance descriptions by quantum field theories is a central topic in theoretical condensed matter physics [1, 2]. Pioneering work on the ground state of spin chains found a striking role is played by the size of the quantum spin [3, 4]: while half integer spins generically realize a gapless critical phase, integer spin chains realize a topological “Haldane phase”. In the field theoretic understanding, the value of the microscopic value of the spin enters as a co-efficient of a topological term that has a dramatic effect on the spin chain phase diagram. Given this profound result in one dimension, it is natural to ask how the value of the spin- S affects the phase diagrams of two dimensional quantum spin systems?

For one dimensional systems, progress in our understanding is largely due to the availability of specialized analytic [5, 6] and numerical methods [7]. These methods cannot be extended as effectively to two dimensions, where consequently much less is known despite intense research. The most reliable unbiased method to study field theory and quantum criticality in two dimensions are limited to models that do not suffer from the sign problem of quantum Monte Carlo [8]. Although the sign-free condition is very restrictive, given their unique ability to provide unbiased insight it is of great interest to build a repertoire of sign-free spin models for arbitrary spin- S , as has been achieved for $S = 1/2$ [9].

In this Letter we develop a systematic method to write down a large family of sign-free bipartite spin models with arbitrary spin- S and multi-spin interactions that have the Heisenberg rotational symmetry. These new models open the door to study a variety of new phases and phase transitions, many of which are of great interest to the community. As a first application of our method we design a square lattice $S = 1$ interaction that realizes a long anticipated “Haldane nematic” (HN) phase [10, 11]. In this phase the spin system breaks lattice rotation symmetry but preserves lattice translations due to the spontaneous formation of Haldane chains either in the x or y direction with an associated two-fold ground state degeneracy, Fig. 1(a). Motivated in part by the Iron

superconductors the HN phase has been under intense study recently (see e.g. [12–15]). An influential work [16] found an exactly solvable model which realizes the HN as a ground state and provided field theoretic arguments for an exotic continuous phase transition to a Néel state described by the $O(4)$ σ -model at $\Theta = \pi$. We establish unambiguously the existence of the HN phase in our new sign free model and provide the first unbiased numerical study of the phase transition from the HN to the Néel state. We find clear evidence that the transition is first order and discuss the implications of this finding for the field theoretic scenario.

Designer Models: While it is well known that the bipartite Heisenberg model is Marshall positive for arbitrary spin- S , what are the most general multi-site spin- S Hamiltonian operators that are sign positive? This question has been difficult to address previously because it appears daunting directly in the language of spin- S operators. Following previous work [17–19] we take a different route – we rewrite the spin- S on each of the N_s lattice sites as $2S$ spin- $1/2$ “mini-spins”,

$$\mathbf{S}_i = \sum_a \mathbf{s}_i^a. \quad (1)$$

We note here that the \mathbf{s}_i^a have both a lattice index i ($1 \leq i \leq N_s$) and a mini-spin index a ($1 \leq a \leq 2S$), giving a total of $2SN_s$ mini-spins. To faithfully simulate the original problem, we have to include a projection operator, $\mathcal{P} = \prod_i \mathcal{P}_i$, where \mathcal{P}_i projects out the spin- S from the \mathbf{s}_i^a basis, $Z = \text{Tr}_{\mathbf{S}} [e^{-\beta H(\mathbf{S})}] = \text{Tr}_{\mathbf{s}} [e^{-\beta H(\mathbf{s})} \mathcal{P}]$. Since \mathcal{P} is itself sign-problem free, in the world-line approach, any model which is sign-free in the \mathbf{s}_i^a basis gives us a sign-free spin- S model!

In this manuscript we illustrate our idea using $S = 1$ spins on the square lattice, but our results can be straightforwardly extended to any bipartite lattice with arbitrary spin- S . Consider first in the \mathbf{s} language the $S = 1$ Heisenberg model,

$$H_2^{ij} = \mathbf{S}_i \cdot \mathbf{S}_j - 1 = - \sum_{a,b} \left(\frac{1}{4} - \mathbf{s}_i^a \cdot \mathbf{s}_j^b \right) \quad (2)$$

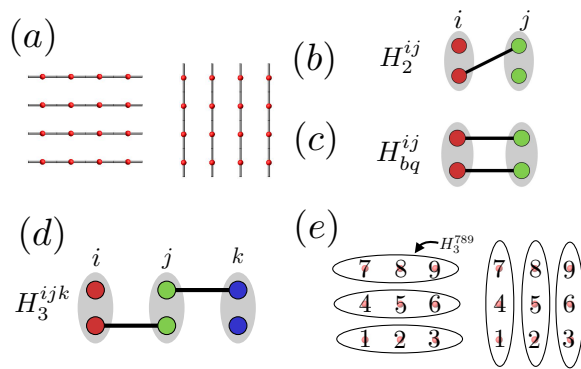


FIG. 1: (a) Two-fold degenerate ground states in the “Haldane nematic” phase for square lattice $S = 1$ spins (red spheres). The strong bonds indicate the spontaneous formation of gapped Haldane chain that breaks lattice rotational symmetry while preserving translations. (b,c,d) Representative mini-spin interaction diagrams that appear in the (b) two-site H_2^{ij} Heisenberg, Eq.(2), (c) the H_{bq}^{ij} biquadratic, and (d) three-site H_3^{ijk} , Eq.(3) interactions. The two mini-spins corresponding to an on-site $S = 1$ are collected in a grey bubble. (e) The $H_{3 \times 3}^p$ interaction acts on the elementary 3×3 plaquette indexed by p . It is constructed out of sum of two terms, each of which is a product of three H_3^{ijk} terms. To preserve square lattice symmetry both the orientations that are shown are included in Eq. (5).

Diagrammatically we can represent each $\frac{1}{4} - \mathbf{s}_i^a \cdot \mathbf{s}_j^b$ term in the sum in the last expression as an “s-bond” between mini-spins a and b on the two sites i and j . A representative such term is illustrated for $S = 1$ with two mini-spins per site in Fig. 1(b) (there are three other such diagrams corresponding to the sum on a, b). Likewise, it is easy to see that the interaction with two s-bonds between i and j corresponds to the sign free region of the biquadratic interaction, Fig. 1(c) [20, 21]. From these examples, we make our central observation – *it is much easier to write down a sign free model in the s language than directly in the spin- S basis*. As a non-trivial example consider interactions between three $S = 1$ spins in a row. In the s-bond language the most natural interaction is with a single bond between each pair of neighbors without allowing them to touch on the middle site, Fig. 1(d). Working backwards we then find this new sign-free interaction in terms of the spin-1 operators is,

$$H_3^{ijk} = -\mathbf{S}_i \cdot \mathbf{S}_j \mathbf{S}_j \cdot \mathbf{S}_k - \mathbf{S}_k \cdot \mathbf{S}_j \mathbf{S}_j \cdot \mathbf{S}_i \quad (3)$$

$$+ \mathbf{S}_i \cdot \mathbf{S}_j + \mathbf{S}_i \cdot \mathbf{S}_k + \mathbf{S}_j \cdot \mathbf{S}_k - 1 \quad (4)$$

For $S = 1$ models the three-site interaction and its physical significance has been discussed recently [22, 23]. Here we discover that in order to study such terms in a sign free way we have to include two spin terms to balance the signs. Using the three-site interaction H_3^{ijk} , we introduce a model interaction we will study in detail below. Following the idea of the J-Q model [24] we construct a

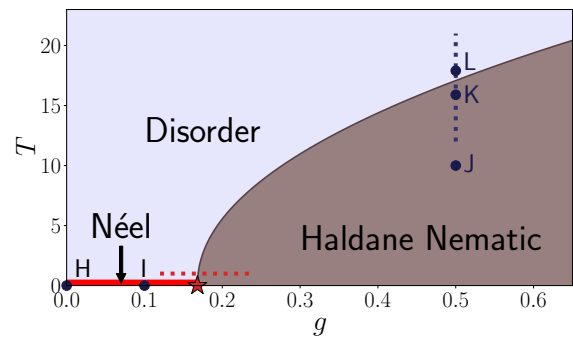


FIG. 2: Phase diagram of the model Eq. (6) in the g - T plane. As we establish by extensive numerical simulations, at $g \approx 0.17$ there is a first order quantum phase transition from Néel to the Haldane nematic (HN) phase. The solid line is a guide to the eye of the phase transition between HN and a simple disordered phase. The solid line is determined as a fit to the location of the transition at a few different g [21] by detailed numerical study (as in Figs. 4,5). The transition is found to be continuous at high- T and first order at low- T (close to the quantum transition), see respectively Fig. 4 (corresponding to the vertical dashed line at $g = 0.5$) & Fig. 5 (the horizontal dashed line at $T = 1$). The (g, T) values for the points labeled in the phase diagram and presented in Fig. 3 are **H**:(0,0) **I**:(0.1,0) **J**:(0.5,10) **K**:(0.5,15.9) **L**:(0.5,17.9)

3×3 plaquette interaction from H_3^{ijk} ,

$$H_{3 \times 3}^p = H_3^{123} H_3^{456} H_3^{789} + H_3^{147} H_3^{258} H_3^{369}, \quad (5)$$

The indexing of the sites in the plaquette by numbers 1-9 is shown in Fig. 1(e). The two terms are included to preserve square lattice symmetry.

We emphasize that in addition to the advantage of leading us to new non-trivial sign free interactions, the mini-spin representation also offers us a simple way to construct efficient loop update algorithms for complex interactions such as Eq. (5), since we can update the s interactions using the standard deterministic algorithm using for e.g. the stochastic series expansion [25]. The update of the symmetrization operator is straightforward [21]. Clearly this program of designing sign-free interactions in terms of the s-bond diagrammatic representation and then into the spin operators can be extended systematically to any value of spin- S and to a wide range of multi-spin interactions. Rather than elaborate on this here, we now turn to an application.

Haldane Nematic: We consider square lattice $S = 1$ antiferromagnets, which have been argued to host an exotic “Haldane nematic” (HN) state in their phase diagrams. Our goal here is to establish that the sign-free model, Eq. 5 realizes this novel phase and carry our unbiased studies of the phase transitions of the destruction of HN order.

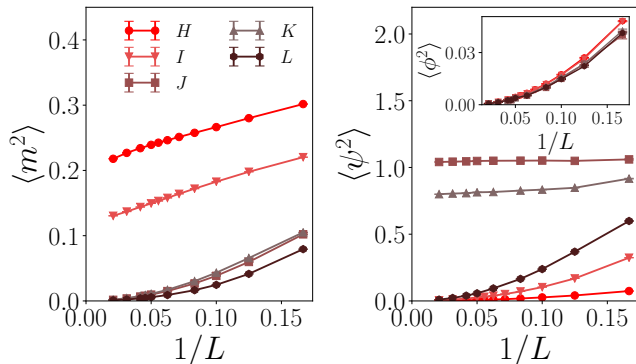


FIG. 3: Extrapolations of the order parameters as a function of $1/L$ for various points labeled in the g - T phase diagram shown in Fig. 2. The left panel shows the Néel order parameter, the right panel shows the order parameter for the Haldane nematic. The inset on the upper right shows the conventional “dimerized” $(\pi, 0)$ VBS order, $\langle \phi^2 \rangle$ that breaks translations as well as rotations, which is found to vanish in the model under study here.

The model we study is,

$$H = J \sum_{\langle ij \rangle} H_2^{ij} + Q_{3 \times 3} \sum_p H_{3 \times 3}^p. \quad (6)$$

The first term is the usual square lattice $S = 1$ Heisenberg model. The second term is our new designer interaction with a sum on p , which runs over the elementary 3×3 plaquettes on the square lattice. We study the phase diagram as a function of $g \equiv Q_{3 \times 3}/J$ and the temperature $T = 1/\beta$. We work in units in which $J^2 + Q_{3 \times 3}^2 = 1$. The phase diagram inferred from our simulations is shown in Fig. 2. At $(g, T) = (0, 0)$ (labelled as **H**) our model is the nearest neighbor $S = 1$ Heisenberg model which is Néel ordered [26]. We use the conventional order parameter $\langle m^2 \rangle$ with $m = \sum_{\mathbf{r}} e^{i(\pi, \pi) \cdot \mathbf{r}} S_{\mathbf{r}}^z / N_s$ to diagnose long range magnetic order. From the finite size scaling of $\langle m^2 \rangle$ we observe that the Néel order weakens as g is increased (**I**). At $T = 0$ the Néel order is stable until we reach a coupling $g \approx 0.17$ at which Néel order is destroyed. As is well known, the Néel order cannot survive finite- T Mermin-Wagner fluctuations in two dimensions.

We now present extensive numerical evidence that at $T = 0$ for $g \geq 0.17$ the system transitions into the “Haldane nematic” phase (Fig. 1(a)). We first rule out a conventional VBS pattern where pairs of $S = 1$ dimerize into a columnar pattern [27], which can be studied by finite size scaling of $\langle \phi^2 \rangle$ with $\phi = \sum_{\mathbf{r}} e^{i(\pi, 0) \cdot \mathbf{r}} B_x(\mathbf{r}) / N_s$ [with the bond operator $B_i(\mathbf{r}) \equiv J \mathbf{S}_{\mathbf{r}} \cdot \mathbf{S}_{\mathbf{r} + \mathbf{e}_i}$]. As shown in the inset of Fig. 3 $\langle \phi^2 \rangle$ scales to zero in the thermodynamic limit indicating that in all parts of the phase diagram under study the conventional VBS order is absent. We use an order parameter [28] $\langle \psi^2 \rangle$ that is sensitive to breaking of rotational symmetry without

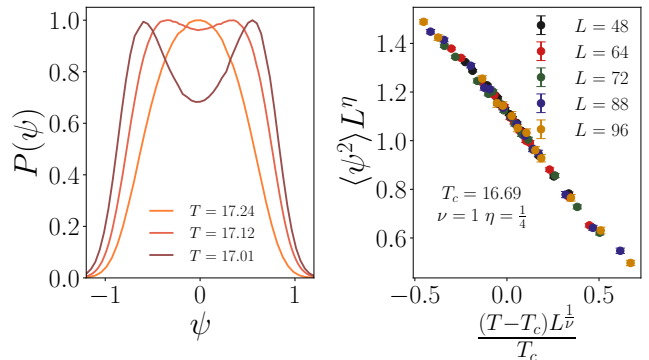


FIG. 4: Behavior of the HN order parameter at the thermal transition at $g = 0.5$, along the vertical dashed line in Fig. 2. The left panel shows the histograms of the order parameter ψ as T is lowered showing the emergence of two symmetry related Ising peaks, and no evidence for first order behavior or phase co-existence. The right panel shows the collapse of the HN order parameter with two dimensional Ising critical exponents, providing further evidence for a two-fold symmetry breaking in the ground state, consistent with Fig. 1(a).

picking up signals of translational symmetry breaking. $\psi = \sum_{\mathbf{r}} (B_x(\mathbf{r}) - B_y(\mathbf{r})) / N_s$. Clearly a condensation of ψ indicates the breaking of lattice rotational symmetry. As shown in Fig. 3 **K** and **J** clearly have long range HN order, whereas at the other points they are absent either because of Néel order (**H** and **I**) or thermal disorder (**L**).

We now turn to a study of the phase transition at which HN order is destroyed. We begin by simulating the model at $g = 0.5$ and tuning T along the vertical dashed line in Fig. 2. From Fig 3, as we move from **L** (no HN order) to **K** (HN order) to **J** (stronger HN order) we have clear evidence for a phase transition. If the pattern of symmetry breaking is of the form Fig. 1(a) thermal criticality is expected to be of the Ising universality class. In Fig. 4 we present a study of the histograms of the order parameter. We see that just above the critical T , $P(\psi)$ shows one peak at zero. As T is lowered, the zero-peak splits into two symmetric peaks corresponding to spontaneous symmetry breaking, just as one expects for the Ising model. There is no evidence for a peak at zero co-existing with the non-zero peaks, which one would expect at a first order transition. A study of the scaling behavior of the T -dependence of the order parameter at $g = 0.5$ (right panel of Fig. 4) shows conclusive evidence that the HN order parameter undergoes a continuous thermal Ising phase transition, as expected for its order parameter manifold. This provides our final piece of evidence that the broken symmetry is indeed of the Haldane nematic form illustrated in Fig. 1(a).

A final interesting question we address is the nature of the quantum phase transition between Néel-HN, labeled by a star in Fig. 2. The field theory for this phase

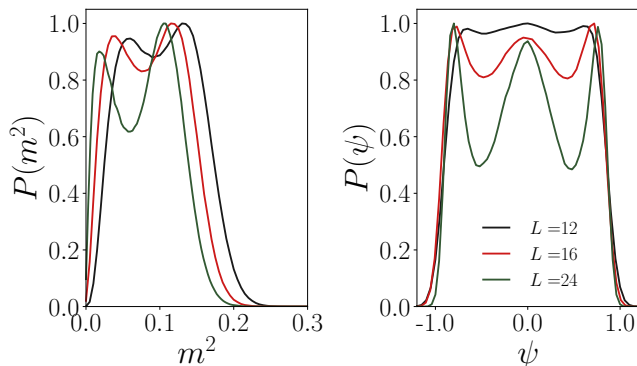


FIG. 5: Evidence for first order behavior at the phase transition at $T = 1$ in Fig. 2. The left panel shows the histogram for m^2 . The right panel shows the histograms for ψ . The data shows that the double peaked behavior clearly gets sharper as the system size, L is increased, indicating that first order behavior persists in the thermodynamic limit.

transition has been argued to be the $O(4)$ σ -model at topological angle π [16], building on previous work for $S = 1/2$ [29, 30]. Very little is known about this field theory, but a consistent scenario for a continuous transition with emergent $O(4)$ symmetry at the critical point would require only one relevant $O(3) \times Z_2$ anisotropy that appears as the tuning parameter g in the lattice model. This delicate question has not yet been accessed in unbiased simulations. To approach this point we study the nature of the phase transition as we move down the thermal phase transition line to lower temperatures. From Fig. 4, we have seen at high- T the transition is continuous and of the Ising type. In Fig. 5 we study data at $T = 1$ (which is very low- T in the units in which we are working) while tuning g (horizontal dashed line in Fig. 2). The histogram data shows clear evidence that the transition has become first order for the HN order parameter, with a co-existence of a peak at zero (for non-HN phase) and the finite symmetry related peaks for the HN phase. While there is no thermal phase transition for the Néel order it also shows double peaks that are incipient behavior of the first order quantum phase transition it undergoes at $g \approx 0.17$. We thus reach the conclusion that along the phase boundary line (solid curve in Fig. 2) the phase transition changes from being Ising and continuous at high- T to becoming first order at low- T and remains first order at the quantum phase transition, marked with a star. The change from continuous Ising to first order is expected to happen at a multi-critical point somewhere along the solid line in Fig. 2 between the two limiting cases we have studied and is expected to be described by the tricritical Ising field theory [31]. We have not made an effort to locate this point precisely in our phase diagram in this work.

Our finding of a first order quantum transition can

be interpreted in two different ways for the $O(4)$ sigma-model at $\theta = \pi$. The first is simply that the field theory itself does not have a non-trivial critical fixed point, the other is that such a fixed point exists but it has more than one relevant $O(3) \times Z_2$ anisotropy and thus requires more than one tuning parameter to be reached. We note that our finding is consistent with previous studies of the $S = 1/2$ Néel-VBS deconfined critical point on a rectangular lattice which is expected to be described by the same field theory and anisotropies as the $S = 1$ Néel-HN studied here [3, 11, 32] and was also found to be first order [33].

Conclusions: We have introduced a scheme to design general multi-spin interactions for spin- S models without the sign problem. Our scheme opens up the possibility to simulate a wide range of models and address the role of S on various quantum phase transitions in two and higher dimensions. As an interesting application of our design procedure we identified a rotationally symmetric $S = 1$ square lattice spin model that realizes a novel Haldane nematic phase. The phase transitions at which HN order was destroyed were studied in detail including the quantum transition from the Néel to HN which was found to be of first order.

Acknowledgments: We gratefully acknowledge useful discussion with S. Pujari and partial support from NSF DMR-1611161 and Keith B. MacAdam Graduate Excellence Fellowship. The numerical results were produced on SDSC comet cluster through the NSF supported XSEDE award TG-DMR140061 as well as the DLX cluster at UK.

-
- [1] S. Sachdev, *Quantum Phase Transitions* (Cambridge University Press, 1999).
 - [2] E. Fradkin, *Field Theories of Condensed Matter Physics* (Cambridge University Press, 2013).
 - [3] F. D. M. Haldane, Phys. Rev. Lett. **61**, 1029 (1988), URL <https://link.aps.org/doi/10.1103/PhysRevLett.61.1029>.
 - [4] I. Affleck, in *Fields, strings, and critical phenomena : 49th Les Houches Summer school of theoretical physics* (North Holland, 1990), pp. 565–640.
 - [5] B. Sutherland, *Beautiful Models* (World Scientific, 2004).
 - [6] T. Giamarchi, *Quantum Physics in One Dimension* (Oxford, 2004).
 - [7] S. R. White, Phys. Rev. Lett. **69**, 2863 (1992), URL <http://link.aps.org/doi/10.1103/PhysRevLett.69.2863>.
 - [8] R. K. Kaul, R. G. Melko, and A. W. Sandvik, Annu. Rev. Cond. Matt. Phys **4**, 179 (2013), URL <http://www.annualreviews.org/doi/abs/10.1146/annurev-conmatphys-030212-184215>.
 - [9] R. K. Kaul, Phys. Rev. B **91**, 054413 (2015), URL <http://link.aps.org/doi/10.1103/PhysRevB.91.054413>.
 - [10] I. Affleck, T. Kennedy, E. Lieb, and H. Tasaki, Commun. Math. Phys. **115**, 477 (1988).
 - [11] N. Read and S. Sachdev, Phys. Rev. B **42**,

- 4568 (1990), URL <https://link.aps.org/doi/10.1103/PhysRevB.42.4568>.
- [12] J.-Y. Chen, S. Capponi, and D. Poilblanc, Phys. Rev. B **98**, 045106 (2018), URL <https://link.aps.org/doi/10.1103/PhysRevB.98.045106>.
- [13] H. C. Jiang, F. Krüger, J. E. Moore, D. N. Sheng, J. Zaanen, and Z. Y. Weng, Phys. Rev. B **79**, 174409 (2009), URL <https://link.aps.org/doi/10.1103/PhysRevB.79.174409>.
- [14] S.-S. Gong, W. Zhu, D. N. Sheng, and K. Yang, Phys. Rev. B **95**, 205132 (2017), URL <https://link.aps.org/doi/10.1103/PhysRevB.95.205132>.
- [15] P. Bilbao Ergueta and A. H. Nevidomskyy, Phys. Rev. B **92**, 165102 (2015), URL <https://link.aps.org/doi/10.1103/PhysRevB.92.165102>.
- [16] F. Wang, S. A. Kivelson, and D.-H. Lee, Nature Physics **11**, 959 EP (2015), URL <http://dx.doi.org/10.1038/nphys3456>.
- [17] S. Todo and K. Kato, Phys. Rev. Lett. **87**, 047203 (2001), URL <https://link.aps.org/doi/10.1103/PhysRevLett.87.047203>.
- [18] N. Kawashima and J. E. Gubernatis, Phys. Rev. Lett. **73**, 1295 (1994), URL <https://link.aps.org/doi/10.1103/PhysRevLett.73.1295>.
- [19] N. Kawashima and K. Harada, Journal of the Physical Society of Japan **73**, 1379 (2004), <https://doi.org/10.1143/JPSJ.73.1379>, URL <https://doi.org/10.1143/JPSJ.73.1379>.
- [20] K. Harada and N. Kawashima, Journal of the Physical Society of Japan **70**, 13 (2001), <https://doi.org/10.1143/JPSJ.70.13>, URL <https://doi.org/10.1143/JPSJ.70.13>.
- [21] Please refer to supplementary materials for more details on the model, numerical test and the details of the QMC simulations.
- [22] F. Michaud and F. Mila, Phys. Rev. B **88**, 094435 (2013), URL <https://link.aps.org/doi/10.1103/PhysRevB.88.094435>.
- [23] N. Chepiga, I. Affleck, and F. Mila, Phys. Rev. B **93**, 241108 (2016), URL <https://link.aps.org/doi/10.1103/PhysRevB.93.241108>.
- [24] A. W. Sandvik, Phys. Rev. Lett. **98**, 227202 (2007), URL <http://link.aps.org/doi/10.1103/PhysRevLett.98.227202>.
- [25] A. W. Sandvik, AIP Conf. Proc. **1297**, 135 (2010), URL <http://scitation.aip.org/content/aip/proceeding/aipcp/10.1063/1.3518900>.
- [26] R. R. P. Singh, Phys. Rev. B **41**, 4873 (1990), URL <https://link.aps.org/doi/10.1103/PhysRevB.41.4873>.
- [27] J. Wildeboer, J. D’Emidio, and R. K. Kaul (2018), URL <https://arxiv.org/abs/1808.04731>.
- [28] T. Okubo, K. Harada, J. Lou, and N. Kawashima, Phys. Rev. B **92**, 134404 (2015), URL <https://link.aps.org/doi/10.1103/PhysRevB.92.134404>.
- [29] A. Tanaka and X. Hu, Phys. Rev. Lett. **95**, 036402 (2005), URL <https://link.aps.org/doi/10.1103/PhysRevLett.95.036402>.
- [30] T. Senthil and M. P. A. Fisher, Phys. Rev. B **74**, 064405 (2006), URL <https://link.aps.org/doi/10.1103/PhysRevB.74.064405>.
- [31] J. Cardy, *Scaling and Renormalization in Statistical Physics* (Cambridge University Press, 1996).
- [32] T. Senthil, A. Vishwanath, L. Balents, S. Sachdev, and M. P. A. Fisher, Science **303**, 1490 (2004), URL <http://www.sciencemag.org/content/303/5663/1490.abstract>.
- [33] M. S. Block, R. G. Melko, and R. K. Kaul, Phys. Rev. Lett. **111**, 137202 (2013), URL <http://link.aps.org/doi/10.1103/PhysRevLett.111.137202>.

SUPPLEMENTAL MATERIALS

Split Spin Representation:

We use the split spin representation [1],[2] to map a model of interacting spin- S 's onto a model of spin- $\frac{1}{2}$'s. In this representation spin- S operators on each site are written as a sum of $2S$ spin- $\frac{1}{2}$ operators (mini-spins) as shown in below:

$$\vec{S}_i = \sum_{\mu=1}^{2S} \vec{s}_i^\mu \quad (7)$$

The partition function of the original spin- S model in terms of the resulting spin- $\frac{1}{2}$ Hamiltonian, \tilde{H} can be written as:

$$Z = \text{Tr}_s(e^{-\beta\tilde{H}}\mathcal{P}) \quad (8)$$

$$\mathcal{P} = \prod_i \mathcal{P}_i \quad (9)$$

where \mathcal{P}_i at each site i acts on the 2^{2S} dimensional Hilbert space spanned by the spin- $\frac{1}{2}$'s and projects out unphysical states that don't belong to the spin- S subspace. \tilde{H} is invariant under exchange of the mini-spin indices at each site and therefore commutes with \mathcal{P} .

Projection Operator

The projection operator has all positive matrix elements and hence can be simulated without a sign problem. Taking the spin-1 case for simplicity, the projection operator is given by:

$$\mathcal{P}_i = |\uparrow\uparrow\rangle\langle\uparrow\uparrow| + |\downarrow\downarrow\rangle\langle\downarrow\downarrow| + \left(\frac{|\uparrow\downarrow\rangle + |\downarrow\uparrow\rangle}{\sqrt{2}}\right)\left(\frac{\langle\uparrow\downarrow| + \langle\downarrow\uparrow|}{\sqrt{2}}\right) \quad (10)$$

The update of this operator in our QMC procedure can be carried out using the directed loop algorithm [3]. Fig. 6 shows the loop updates with their respective probabilities for this operator.

The loop update in Fig. 6 can be generalized to higher spins as follows: the loop entering the operator continues in the same direction exiting on any mini-spin who's state is the same as that of the mini-spin at which it entered. The operator can also be thought of as a "soft" boundary condition in the imaginary time direction. The spin- S state is the highest spin that can be gotten from the sum on $2S$ spin- $\frac{1}{2}$'s and the highest spin state wavefunction has to be completely symmetric in the mini-spins. Hence, the \mathcal{P}_i operator is identical to a local symmetrization operator at site i . It ensures that the Hamiltonian

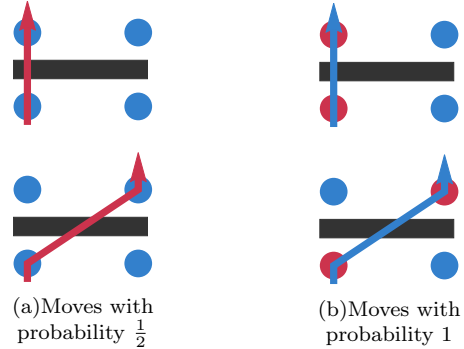


FIG. 6: Loop moves to update the projection operator. The two colors represent the two spin states, a loop update flips the spin to a different state. (b) are equivalent to the reverse moves of (a)

operators propagate the spin state in the imaginary time (τ) direction so that the spin state at $\tau = \beta$ is the spin state at $\tau = 0$ upto a permutation of the $2S$ mini-spins at each site.

Designer Hamiltonians:

Consider the spin- S nearest neighbour Heisenberg Antiferromagnet (upto a constant, $-S^2$) on a bipartite lattice,

$$\begin{aligned} H &= -J \sum_{\langle ij \rangle} (S^2 - \vec{S}_i \cdot \vec{S}_j) \\ &= J \sum_{\langle ij \rangle} H_{ij} \end{aligned} \quad (11)$$

where

$$H_{ij} = \vec{S}_i \cdot \vec{S}_j - S^2 \quad (12)$$

By carrying out a Unitary transformation of the spin operators on one of the sublattices such that $S_i^+ \rightarrow -S_i^-$ and $S_i^- \rightarrow -S_i^+$, one can easily see that the operator H_{ij} has all negative matrix elements. This can be simulated without a sign problem using QMC. This is because the Hamiltonian enters the series expansion of the partition function as powers of $-\beta H$ giving a positive probability for each term in the partition function [4]. For the spin- $\frac{1}{2}$ case this quantity $P_{ij} = \frac{1}{4} - \vec{S}_i \cdot \vec{S}_j$ is a singlet projection operator. All models constructed out of P_{ij} , e.g. products of P_{ij} on two bonds on a plaquette, are sign problem-free. We use this fact to construct designer Hamiltonians for arbitrary S as described in the main manuscript.

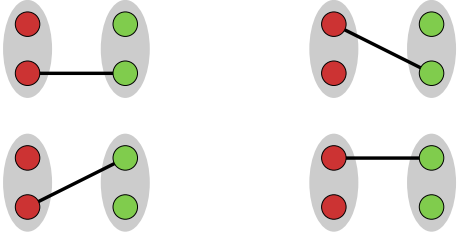


FIG. 7: Each gray bubble with two circles represents two spin- $\frac{1}{2}$'s at each spin-1 site. The black line is the operator P_{ij} acting on the two mini-spins. The four diagrams denote the four terms in the summation in Eq. 13

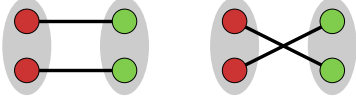


FIG. 8: These two diagrams is equivalent to the first two terms in the square bracket in Eq. 15

In terms of spin- $\frac{1}{2}$'s H_{ij} can be written as:

$$\tilde{H}_{ij} = -J \sum_{a,b=1}^{2S} \left(\frac{\mathbb{1}}{4} - \vec{s}_i^a \cdot \vec{s}_j^b \right) \quad (13)$$

The above spin- $\frac{1}{2}$ Hamiltonian is a sum of four terms, each of which can be depicted pictorially as in Fig. 7. Similarly, the biquadratic term given by H_{biquad} in Eq. 14 can be expressed in terms of the mini-spins as \tilde{H}_{biquad} as in equation 15. The last two terms colored in red in Eq. 15 get killed by the action of the projection operator \mathcal{P} at each of these sites. This is because these operators are singlet projection operators on the two mini-spins at the same site. This operator is anti-symmetric in these two mini-spins and therefore gets cancelled by the symmetrization operator \mathcal{P} . The remaining two terms in Eq. 15 can be understood more easily with the help of Fig. 8

$$H_{biquad} = (\vec{S}_i \cdot \vec{S}_j)^2 - \mathbb{1} \quad (14)$$

$$\begin{aligned} \tilde{H}_{biquad} = \sum_{a,b=1}^2 & \left[\left(\frac{\mathbb{1}}{4} - \vec{s}_i^a \cdot \vec{s}_j^a \right) \cdot \left(\frac{\mathbb{1}}{4} - \vec{s}_i^b \cdot \vec{s}_j^b \right) + \right. \\ & \left. \left(\frac{\mathbb{1}}{4} - \vec{s}_i^a \cdot \vec{s}_j^b \right) \cdot \left(\frac{\mathbb{1}}{4} - \vec{s}_i^b \cdot \vec{s}_j^a \right) + \right. \\ & \left. \frac{1}{2} \left(\vec{s}_i^a \cdot \vec{s}_i^b - \frac{\mathbb{1}}{4} \right) + \frac{1}{2} \left(\vec{s}_j^a \cdot \vec{s}_j^b - \frac{\mathbb{1}}{4} \right) \right] \quad (15) \end{aligned}$$

We now construct a sign problem-free interaction symmetric in the mini-spins at each site, directly in the spin- $\frac{1}{2}$ language. This simple construction involves three neighbouring sites. A singlet projection operator acts on each

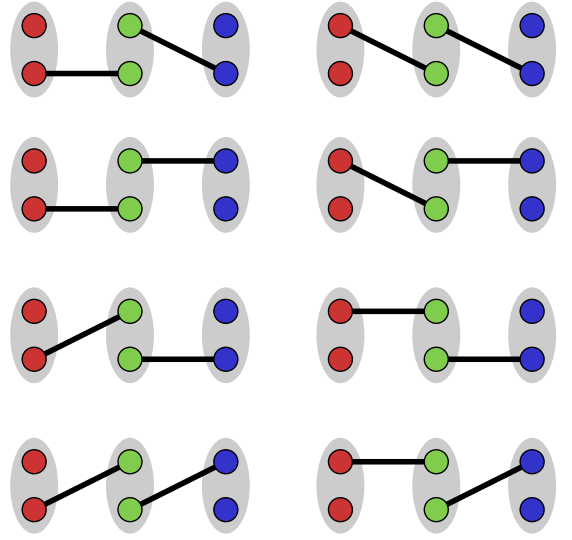


FIG. 9: Interaction between three spin-1's in terms of the mini-spins

pair of neighbouring spin- $\frac{1}{2}$'s on the three sites, such that none of these singlets touch. The 8 possible ways to form singlets on three sites in this manner are shown in Fig. 9

The Hamiltonian described by Fig. 9 is written down in Eq. 16.

$$\tilde{H}_{int} = - \sum_{\langle ijk \rangle} \sum_{a,d,b \neq c} \left(\frac{\mathbb{1}}{4} - \vec{s}_i^a \cdot \vec{s}_j^b \right) \left(\frac{\mathbb{1}}{4} - \vec{s}_j^c \cdot \vec{s}_k^d \right) + h.c. \quad (16)$$

This interaction always involves four spin- $\frac{1}{2}$'s, because interactions involving three spin- $\frac{1}{2}$'s like the ones shown in Fig. 10 can be shown to reduce to two spin interactions.

We now proceed to work out this interaction in terms of the original spin-1 operators.

$$\begin{aligned} \tilde{H}_{int} &= - \sum_{\langle ijk \rangle} \sum_{a,d,b \neq c} \left(\frac{\mathbb{1}}{4} - \vec{s}_i^a \cdot \vec{s}_j^b \right) \left(\frac{\mathbb{1}}{4} - \vec{s}_j^c \cdot \vec{s}_k^d \right) \\ &= - \sum_{\langle ijk \rangle} \left[\sum_{a,b,c,d} \left(\frac{\mathbb{1}}{4} - \vec{s}_i^a \cdot \vec{s}_j^b \right) \left(\frac{\mathbb{1}}{4} - \vec{s}_j^c \cdot \vec{s}_k^d \right) \right. \\ & \quad \left. - \sum_{a,b,c} \left(\frac{\mathbb{1}}{4} - \vec{s}_i^a \cdot \vec{s}_j^b \right) \left(\frac{\mathbb{1}}{4} - \vec{s}_j^b \cdot \vec{s}_k^c \right) \right] \quad (17) \end{aligned}$$

In the square bracket in the last line of Eq. 17:

- the first term is the sum of all the terms in Fig. 9 and Fig. 10
- the second term is a sum on all the terms in Fig. 10

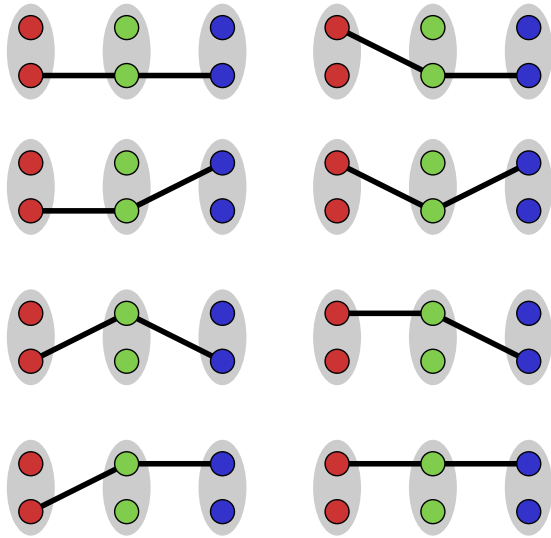


FIG. 10: Interactions involving three spin- $\frac{1}{2}$'s, the middle spin squares to 1 resulting in a net two spin interaction

The two terms are not individually Hermitian, so they are first added to their corresponding Hermitian conjugates before simplifying to get H_{int}^d and $H_{int}^{d'}$ respectively in Eq. 18 .

$$\begin{aligned}
 H_{int}^d &= - \sum_{\langle ijk \rangle} (\mathbb{1} - \vec{S}_i \cdot \vec{S}_j)(\mathbb{1} - \vec{S}_j \cdot \vec{S}_k) + h.c. \\
 H_{int}^{d'} &= \sum_{\langle ijk \rangle} (\vec{S}_i \cdot \vec{S}_j + \vec{S}_j \cdot \vec{S}_k - \vec{S}_i \cdot \vec{S}_k - \mathbb{1})
 \end{aligned} \tag{18}$$

Finally, our constructed three spin interaction in terms of the spin-1's

$$\begin{aligned}
 H_{int} &= H_{int}^d + H_{int}^{d'} \\
 &= -\vec{S}_i \cdot \vec{S}_j \vec{S}_j \cdot \vec{S}_k + \frac{1}{2}(\vec{S}_i \cdot \vec{S}_j + \vec{S}_i \cdot \vec{S}_k + \vec{S}_j \cdot \vec{S}_k + 2) + h.c.
 \end{aligned} \tag{19}$$

as in Eq. 3, 4 in the main manuscript.

Measurements

Here we outline the order parameters that we used to characterize the different phases:

1. The spin spin correlation function is used to identify the magnetic order. The Fourier transform of $\langle S^z(\vec{0})S^z(\vec{r}) \rangle$ has a Bragg peak at the $\vec{k} = (\pi, \pi)$, the height of this peak is our order parameter $\langle m^2 \rangle$ [5].

Lattice	Lx	Ly	S	e_{ED}	e_{QMC}	ρ_s^{ED}	ρ_s^{QMC}
Square	4	4	$\frac{1}{2}$	-1.20178	-1.20186(8)	0.1855	0.1849(4)
Square	2	2	1	-5.0	-5.0011(5)	1.0	1.002(2)
Square	2	2	$\frac{3}{2}$	-10.5	-10.499(5)	2.0	2.008(3)
Chain	4	1	1	-2.5	-2.5004(2)	0.2222	0.2226(4)
Chain	6	1	$\frac{3}{2}$	-5.1488	-5.1489(3)	0.2630	0.2627(3)

TABLE I: Quantities measures by QMC at low temperatures (inverse temperature of $\beta = 6L$) for the Heisenberg Antiferromagnet with coupling constant $J = 1$ compared with those determined for the ground state of the same model as found from Exact Diagonalization (ED). The energies reported (e_{ED} and e_{QMC}) are per site and the stiffness (ρ_s^{ED} and ρ_s^{QMC}) are as described by Eq. 21. The energy saturates to the ground state value for low enough temperatures as can be seen in Fig. 12

2. The spin stiffness defined by Eq. 20 is another quantity used to detect the magnetic phase

$$\rho_s = \left. \frac{\partial^2 E(\phi)}{\partial \phi^2} \right|_{\phi=0} \tag{20}$$

Here $E(\phi)$ is the energy of the system when you add a twist of ϕ in the boundary condition in either the x or the y direction. In the QMC, this quantity is related to the winding number of loops in the direction that the twist has been added:

$$\rho_s = \frac{\langle W^2 \rangle}{\beta} \tag{21}$$

where β is the inverse temperature

3. The correlation function of the singlet projection operator between neighbouring spins, $B_i(\vec{r})$ (Eq. 22), helps determine the presence of the Valence Bond Solid (VBS) order.

$$B_i(\vec{r}) = \sum_{a,b} \left(\frac{1}{4} - \vec{s}_{\vec{r}}^a \cdot \vec{s}_{\vec{r}+i}^b \right) \tag{22}$$

where $i = \hat{x}$ or \hat{y} . A Bragg peak in the Fourier transform of $J \langle B_i(\vec{0})B_i(\vec{r}) \rangle$ (where J is the Heisenberg coupling) at $\vec{k} = (\pi, 0)$ or $\vec{k} = (0, \pi)$ indicates VBS order on the square lattice. The height of this peak is the VBS order parameter given by $\langle \phi^2 \rangle$

4. The Haldane Nematic phase is characterized by long range order in the quantity $\psi(\vec{r})$ which is locally defined at a site as $\psi(\vec{r}) = B_{\hat{x}}(\vec{r}) - B_{\hat{y}}(\vec{r})$. We define our order parameter for this phase by the height of the Bragg peak in the Fourier transform of $J \langle \psi(\vec{0})\psi(\vec{r}) \rangle$ (where J is the Heisenberg coupling) at the $\vec{k} = (0, 0)$.

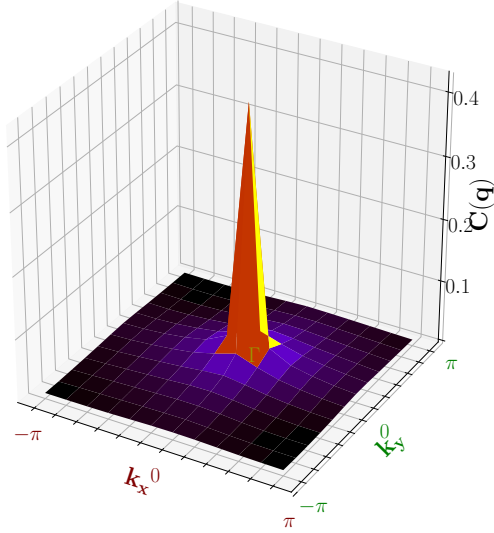


FIG. 11: Fourier transform of $\tilde{C}(r) = \langle \psi(0)\psi(\vec{r}) \rangle$, showing a Bragg peak at Γ in the Haldane Nematic Phase.

Order Parameter Collapses

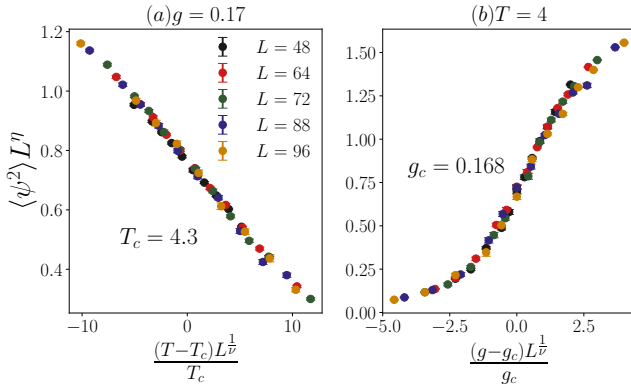


FIG. 15: Order parameter scaling collapse with Ising critical exponents ($\nu = 1$ and $\eta = \frac{1}{4}$) for transitions as a function of (a) temperature for a fixed g and (b) g for a fixed temperature for the model described by Eq. 6 of main manuscript

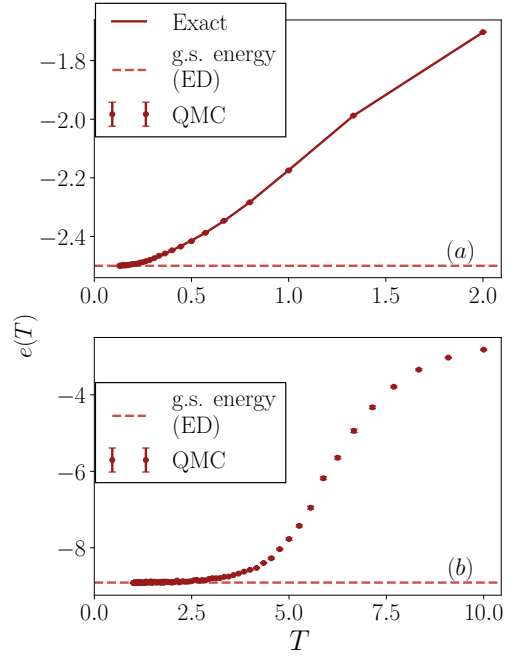


FIG. 12: (a) Finite temperature energy (per unit site) comparison with ED for a 4 site spin-1 Heisenberg Antiferromagnetic chain (b) Ground state energy (per unit site) comparison for a 3×3 square lattice with periodic boundary conditions (PBC) for the model described by a modified version of Eq. 6 of the main manuscript where $S_i \cdot S_j$ replaced by $S_i^z S_j^z - \frac{1}{2}(S_i^+ S_j^+ + S_i^- S_j^-)$ for $g = 0.1$. On a bipartite lattice, this modification corresponds to a unitary transformation on one sublattice and hence simulating the modified model is no different from simulating the original model. However, since the 3×3 square lattice is non-bipartite, it is really the modified model that we simulate in QMC

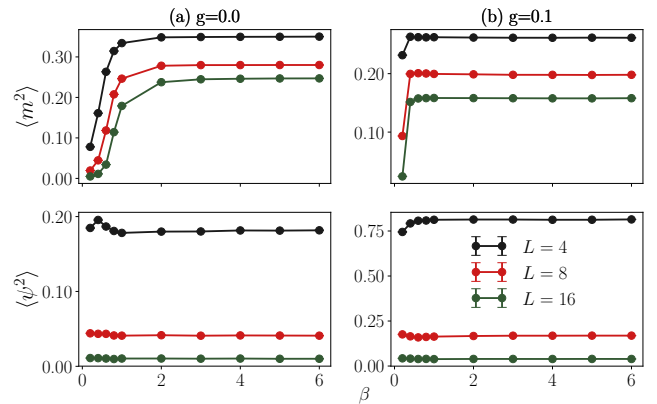


FIG. 13: Convergence of the order parameters ($\langle m^2 \rangle$ and $\langle \psi^2 \rangle$) as a function of inverse temperature for (a) $g = 0.0$ (b) $g = 0.1$: Finite temperature effects are clearly absent for $\beta \geq 4$, therefore we pick $\beta = 4$ for our simulations to study behaviour in the zero temperature limit.

- [1] S. Todo and K. Kato, Phys. Rev. Lett. **87**, 047203 (2001), URL <https://link.aps.org/doi/10.1103/PhysRevLett.87.047203>.
- [2] N. Kawashima and J. E. Gubernatis, Phys. Rev. Lett. **73**, 1295 (1994), URL <https://link.aps.org/doi/10.1103/PhysRevLett.73.1295>.
- [3] O. F. Syljuåsen and A. W. Sandvik, Phys. Rev. E **66**, 046701 (2002), URL <https://link.aps.org/doi/10.1103/PhysRevE.66.046701>.

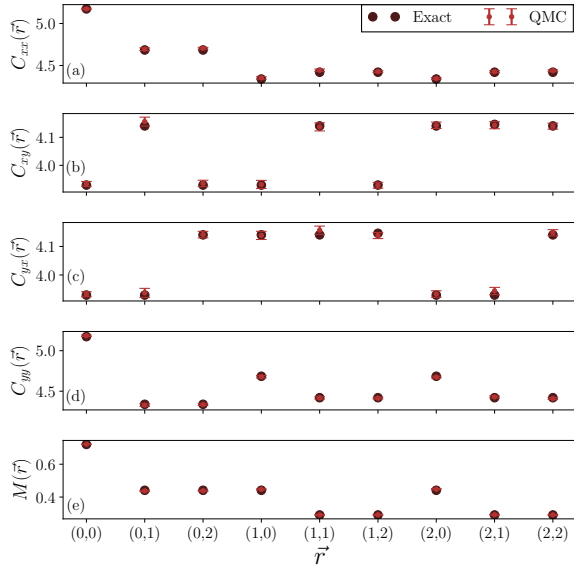


FIG. 14: Correlation function comparison for a 3×3 square lattice with periodic boundary conditions (PBC) for a modified version of the model described by Eq. 6 of the main manuscript for $g = 0.1$ (the modification is as described in the caption of Fig. 12):- (a)-(d): $C_{ij}(\vec{r}) = \langle B_i(0)B_j(\vec{r}) \rangle$ where B_i is the singlet projection operator along the bond oriented in the $i (= \hat{x}/\hat{y})$ direction (e) $M(r)$ is the magnetic correlation function

[1103/PhysRevE.66.046701](https://arxiv.org/abs/1103/PhysRevE.66.046701).

- [4] A. W. Sandvik, in *American Institute of Physics Conference Series*, edited by A. Avella and F. Mancini (2010), vol. 1297 of *American Institute of Physics Conference Series*, pp. 135–338, 1101.3281.
- [5] We define our Fourier transforms so that our order parameters are intensive